

V-Bridge: Bridging Video Generative Priors to Versatile Few-shot Image Restoration

Shenghe Zheng^{1*}, Junpeng Jiang^{2*}, and Wenbo Li^{3†}

¹ The Hong Kong University of Science and Technology

² Harbin Institute of Technology, Shenzhen

³ The Chinese University of Hong Kong

shenghez.zheng@gmail.com, jjunpeng1122@outlook.com, fenglinglwb@gmail.com

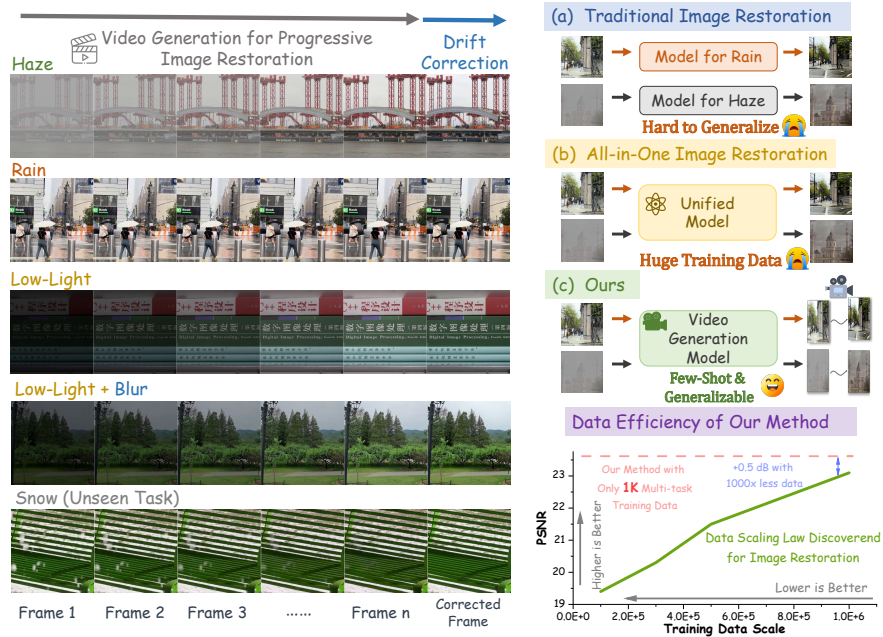


Fig. 1: Left: Image restoration is formulated as progressive video generation with frame drift correction. Right: Leveraging video generative priors leads to stronger generalization under limited data compared to current image restoration method [25].

Abstract. Large-scale video generative models are trained on vast and diverse visual data, enabling them to internalize rich structural, semantic, and dynamic priors of the visual world. While these models have demonstrated impressive generative capability, their potential as general-purpose visual learners remains largely untapped. In this work, we introduce V-Bridge, a framework that bridges this latent capacity to versatile few-shot image restoration tasks. We reinterpret image restoration not as a static regression problem, but as a progressive generative process, and leverage video models to simulate the gradual refinement from

* Equal Contribution. † Corresponding Author. Open-source project: V-Bridge.

degraded inputs to high-fidelity outputs. Surprisingly, with only 1,000 multi-task training samples (less than 2% of existing restoration methods), pretrained video models can be induced to perform competitive image restoration, achieving multiple tasks with a single model, rivaling specialized architectures designed explicitly for this purpose. Our findings reveal that video generative models implicitly learn powerful and transferable restoration priors that can be activated with only extremely limited data, challenging the traditional boundary between generative modeling and low-level vision, and opening a new design paradigm for foundation models in visual tasks.

Keywords: Video Generation · Image Restoration · Prior Transfer

1 Introduction

Large-scale video generative models have recently emerged as powerful visual models [14,39,42]. Trained on massive and diverse video corpora, they internalize not only appearance statistics but also structural regularities, object dynamics, lighting variations, and long-range spatio-temporal coherence. Although primarily optimized for video synthesis, the scale, diversity, and structural richness of their training data imply that these models encode far more general visual priors. Such priors extend beyond generation and suggest substantial untapped potential for a wide range of visual understanding and reconstruction tasks.

Among these visual problems, image restoration [3] remains largely confined to task-specific modeling. From denoising to deblurring, dominant approaches rely on carefully engineered architectures trained with substantial supervision for each degradation type [20, 27, 41]. Despite their efficacy, these paradigms remain decoupled from the rapid advances in generative modeling that have redefined high-level vision. Consequently, they necessitate massive supervision, even exceeding a million samples [25], to learn restoration from scratch for each degradation. This data-intensive approach underutilizes the rich, transferable priors already embedded within large-scale generative models.

In this work, we reimagine the conventional methodology by recasting image restoration as a video generation process, simulating progressive restoration dynamics instead of performing static, one-step regression. Specifically, the degraded image is treated as the initial state, while the high-fidelity reconstruction serves as the terminal point along a quality-refinement trajectory. This formulation allows extensive video generation priors to be seamlessly and efficiently integrated into image restoration tasks, potentially alleviating the massive data requirements typical of traditional paradigms.

Driven by this perspective, we introduce V-Bridge (Fig. 2), a framework that harnesses video generative priors for versatile few-shot image restoration, requiring less than 2% of the training data typical of contemporary methods. V-Bridge models image restoration as a step-wise quality evolution toward high-fidelity outputs. To bridge the resolution gap between moderate-resolution video pretraining and high-resolution restoration, we propose a coarse-to-fine training

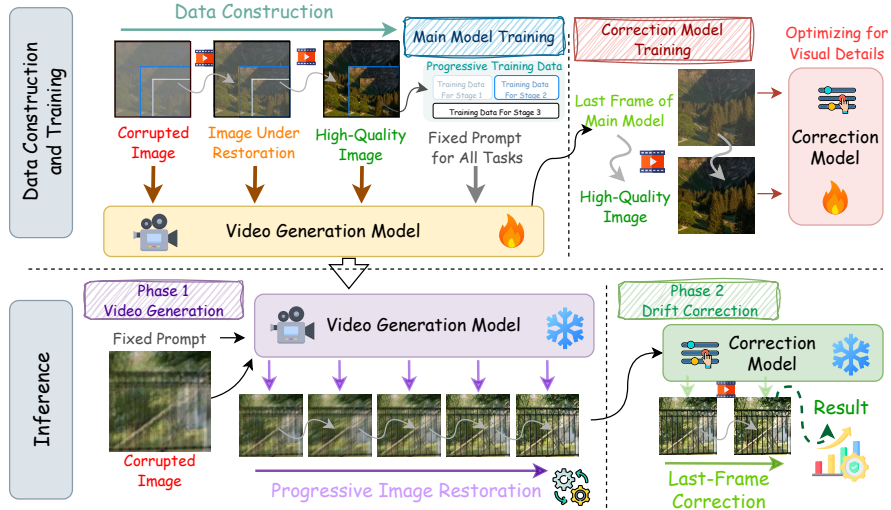


Fig. 2: Overview of the proposed pipeline. The upper part shows data construction and training, where paired low- and high-quality images are used to build pseudo-temporal sequences for progressive restoration learning. A progressive resolution training strategy is adopted to improve fine-grained detail modeling, and an auxiliary generative model is trained for final-frame correction. The lower part shows inference, where the model generates a restoration trajectory and uses the refined last frame as the final output.

curriculum that progressively optimizes the model across increasing scales. This strategy allows the model to first establish global structural coherence before refining high-frequency details, thereby ensuring computational efficiency. Furthermore, we incorporate a drift correction module with minimal overhead to enhance fine-grained texture and color fidelity. Extensive experiments demonstrate that V-Bridge transforms a single video generation model into a versatile restoration expert with only 1,000 multi-task training samples. Our approach achieves a 1.6dB gain over baselines trained on $15\times$ to $1,000\times$ more data. Remarkably, as shown in Fig. 1, V-Bridge generalizes effectively to unseen tasks, showcasing superior out-of-distribution adaptability. Our work opens a new avenue for leveraging rich video priors in low-level vision, paving the way for more general and versatile unified visual models.

Our contributions are threefold:

- **New Restoration Paradigm:** We pioneer the use of video generative models as universal priors, demonstrating that their inherent representations serve as a powerful, transferable foundation across diverse low-level tasks.
- **The V-Bridge Framework:** We propose V-Bridge, a framework designed for data-efficient image restoration via progressive generative refinement. We introduce a coarse-to-fine training curriculum together with a lightweight drift correction mechanism, enabling sophisticated quality enhancement with minimal task-specific supervision.

- **Empirical Validation:** Extensive evaluations reveal that V-Bridge achieves state-of-the-art results with extreme data sparsity (using only 1K samples). Our findings validate the extraordinary out-of-distribution adaptability of video priors and point toward a unified future for low-level modeling.

2 Related Work

2.1 Video Generation

With the success of diffusion models, an increasing number of studies have extended them to video generation. Early approaches typically adopted UNet-based architectures with 2D VAE [4, 7, 19]. However, these designs struggled to achieve substantial performance breakthroughs in terms of scalability and temporal coherence. Inspired by the strong scalability demonstrated by Sora [5], the field has shifted toward large-scale video generation models built upon 3D VAE and Diffusion Transformers (DiT) [35]. State-of-the-art systems now include a series of open-source models such as OpenSora [47], HunyuanVideo [22], and Wan [39], as well as commercial models including Kling [23], Seedance [14], and Veo [15]. Notably, recent advances from Veo and Seedance demonstrate remarkable capability in producing temporally consistent and semantically realistic video content. These developments suggest that video generative models are evolving beyond content synthesis, showing strong potential as general visual foundation models for unified representation learning across diverse vision tasks.

2.2 All-in-One Image Restoration

Traditional image restoration methods are typically designed for a single predefined degradation type, such as motion blur, rain streaks, or noise, requiring separate models for different corruption scenarios [13, 17, 21, 28]. While effective within narrow settings, these task-specific designs limit scalability and practical deployment. All-in-one image restoration aims to handle diverse degradations within a single unified model. Early efforts focused on degradation-aware representation learning, where AirNet [24] utilizes contrastive learning and methods like PromptIR [36] and ProRes [33] introduce lightweight, learnable visual prompt modules to dynamically adapt the network to specific input conditions. To further refine this process, Perceive-IR [45] leverages multi-level quality-driven prompt for fine-grained quality control across various degradation types and severity levels. Diffusion-based frameworks such as DiffUIR [46] and DiffBIR [29] have been introduced to leverage generative priors for higher perceptual quality. Advanced models like AutoDIR [20] and InstructIR [11] further involve the continuous guidance of image restoration via human language instructions. However, these approaches still typically require large-scale training and do not fully exploit large-scale visual priors. In contrast, our work explores restoration from the perspective of leveraging pretrained video generative priors as a general visual prior, enabling progressive quality refinement without designing separate restoration models for each degradation type.

2.3 Chain-of-Frames Reasoning

The rapid maturation of video generation models has catalyzed a paradigm shift from simple motion synthesis to complex visual inference, a phenomenon encapsulated by the Chain-of-Frames (CoF) reasoning [42]. To systematically quantify this emergent intelligence, a diverse array of empirical studies and specialized benchmarks has been established, scrutinizing model performance across dimensions such as spatial relationships, logical reasoning, action planning, and physical dynamics [12, 18, 26, 30, 44]. Parallel to these evaluative efforts, recent advancements have focused on augmenting the CoF reasoning capabilities of video models through supervised fine-tuning (SFT) on curated video sequences [43] and test-time prompt optimization [8]. More recently, the versatility of CoF reasoning has been extended to text-to-image synthesis, yielding promising results by treating image generation as the final-state of a reasoning chain [37]. However, while existing literature predominantly focuses on high-level semantic and logical orchestration, the potential of CoF-driven temporal priors to address low-level vision tasks remains a conspicuously unmapped frontier. This leaves a significant research gap: the question of whether the structured *visual thinking* inherent in CoF can be harnessed to resolve granular pixel-level challenges or restore fine-grained structural integrity remains entirely unexplored.

3 Methodology

3.1 Overview

In this section, we present V-Bridge, a progressive restoration framework that repurposes pretrained video generative priors for image-to-image translation. Unlike vanilla one-step regression, we reformulate restoration as a temporally evolving trajectory that iteratively refines image quality. By harnessing the inherent spatio-temporal consistency and generative priors of video generation models, V-Bridge achieves remarkable performance with only 0.1% to 2% of the task-specific training data required by current methods [20, 25].

The methodology is organized as follows: Sec. 3.2 details the construction of pseudo-temporal sequences from paired low-quality (LQ) and high-quality (HQ) images. Sec. 3.3 presents a Progressive Curriculum Training strategy that transitions from structural recovery to fine-grained synthesis. Finally, Sec. 3.4 describes a Drift Correction mechanism designed to bridge the resolution gap between video generative priors and high-resolution restoration. Through this dynamic formulation, we transform static restoration into a learnable flow problem, fully unlocking the few-shot potential of video foundation models.

3.2 Pseudo-Temporal Data Construction

To translate static restoration into a dynamic generation task, we lift each low-quality-high-quality (LQ-HQ) pair $(\mathbf{I}_{LQ}, \mathbf{I}_{HQ})$ into a pseudo-temporal sequence with explicit quality progression.

Given \mathbf{I}_{LQ} as the anchor (initial frame) and \mathbf{I}_{HQ} as the target (terminal frame), we construct a sequence $\{\mathbf{I}_t\}_{t=0}^T$ of length $T + 1$ such that:

$$\mathbf{I}_0 = \mathbf{I}_{\text{LQ}}, \quad \mathbf{I}_T = \mathbf{I}_{\text{HQ}}. \quad (1)$$

For intermediate frames $t \in \{1, \dots, T - 1\}$, we define a continuous transition path in pixel space via linear interpolation:

$$\mathbf{I}_t = (1 - \alpha_t)\mathbf{I}_{\text{LQ}} + \alpha_t\mathbf{I}_{\text{HQ}}, \quad \alpha_t = \frac{t}{T}. \quad (2)$$

This formulation encapsulates a monotonic quality evolution, providing temporally consistent supervision that guides the model to learn a stable low-to-high quality trajectory. By converting static pairs into a pseudo-video stream, we provide the video model with temporally consistent supervision, enabling it to learn the entire restoration trajectory rather than a singular mapping.

3.3 Progressive Curriculum Training

In this section, we introduce a multi-stage training strategy for efficient and effective restoration. The overall optimization objective remains identical across all stages and follows a supervised fine-tuning paradigm, where the model learns to regress the constructed progressive data sequences. The stage-wise design does not modify the objective itself, but progressively improves the model’s ability to synthesize fine details and enhance fidelity.

Overall Training Objective. Formally, let $\{\mathbf{I}_t\}_{t=0}^T$ denote the pseudo-temporal sequence and θ the model parameters. Given the conditional input \mathbf{I}_0 and the time index t , the model predicts $\hat{\mathbf{I}}_t = f_\theta(\mathbf{I}_0, t)$. The training objective is:

$$\mathcal{L}(\theta) = \mathbb{E}_{(\mathbf{I}_0, \mathbf{I}_t)} [\ell(f_\theta(\mathbf{I}_0, t), \mathbf{I}_t)], \quad (3)$$

where $\ell(\cdot, \cdot)$ denotes a reconstruction loss. This formulation encourages the video model to mimic the image restoration process by progressively approximating the intermediate states, thereby fully unleashing its potential for restoration tasks while learning the complete low-to-high quality trajectory.

Curriculum Training. A key gap between image restoration and video generation lies in training resolution: existing video generative models are rarely trained on high-resolution data (e.g., 4K), which is crucial for fine-detail restoration. However, directly training at such resolutions is computationally expensive and may reduce learning efficiency due to the pre-training–fine-tuning data gap.

To overcome this, we construct a progressive resolution curriculum $\{r_t\}_{t=1}^T$, which controls the difficulty of restoration learning by modulating spatial fidelity across training stages. Let $\{v_i\}_{i=1}^N$ denote the training corpus, where each video $v_i = \{f_{i,1}, \dots, f_{i,T_i}\}$ is a spatio-temporal sample from the video distribution. Instead of training on the original high-resolution data, we apply stage-dependent downsampling. At stage t , video samples are re-encoded using a resolution-aware degradation operator as following:

$$v_i^{(t)} = \text{DownUp}(v_i, r_t), \quad r_t \in \{r_1, r_2, \dots, r_T\}, \quad r_1 < r_2 < \dots < r_T. \quad (4)$$

In simple terms, the video resolution is gradually increased during training. This enables the model to first capture global restoration at low resolution and then progressively enhance fine-grained detail generation as resolution grows.

From a generative modeling perspective, this progressive learning strategy discretizes a continuous restoration probability flow by learning conditional transition kernels across quality levels. By gradually increasing resolution complexity, the model captures hierarchical semantics and high-frequency perceptual statistics in a coarse-to-fine manner, improving few-shot generalization while preserving perceptual fidelity and temporal consistency.

3.4 Drift Correction

The proposed curriculum training reduces cost and optimization difficulty but cannot fully bridge the large gap between pretraining resolution and the fine-grained detail generation capability required in our task. Most video generation models are pretrained at moderate resolutions (e.g., 720p), whereas practical restoration tasks often require recovering ultra high-resolution content (e.g., 4K). This discrepancy limits the model’s ability to faithfully recover high-quality fine details, often leading to struggles in reconstructing high-frequency structures.

We interpret this limitation as an implicit distribution drift induced by the resolution-constrained generative prior. Let \hat{x} denote the final restored frame predicted by the base video generation model, and let x^{HR} denote the corresponding ground-truth high-resolution image. Due to the pretrained resolution bias, \hat{x} exhibits a systematic drift from the target high-fidelity manifold, and can be viewed as a sample drawn from a lower-fidelity distribution:

$$\hat{x} \sim p_{\theta}^{\text{LR}}(x), \quad x^{\text{HR}} \sim p_{\text{HR}}(x), \quad (5)$$

where p_{θ}^{LR} represents the distribution distorted by low-resolution pretraining.

To mitigate this drift, we introduce an additional drift correction model that explicitly learns a short corrective trajectory from \hat{x} toward x^{HR} . The training samples are constructed as short pseudo-temporal sequences interpolating between the drifted base model output and the ground-truth high-quality image, enabling a smooth transition from resolution-limited restoration to full-fidelity reconstruction. We view this transformation as a form of degradation type tailored to the unique characteristics of video generative models.

The drift correction model is trained to parameterize this conditional generative transition, effectively modeling a mapping:

$$g_{\phi} : p_{\theta}^{\text{LR}}(x) \rightarrow p_{\text{HR}}(x), \quad (6)$$

such that the final output approximates x^{HR} while preserving structural consistency with \hat{x} . By restricting the trajectory to only a few intermediate frames, the correction process remains computationally efficient, yet substantially eliminates the resolution-induced bias and enhances perceptual quality.



Fig. 3: Visualization results on a subset of the FoundIR test set. FoundIR-G is the generalist model of FoundIR. GT denotes ground truth. Bounding boxes with different colors indicate zoomed regions for detailed comparison. Compared with other methods, our approach achieves higher visual fidelity and stronger structural consistency, while showing superior robustness across diverse degradation patterns.

4 Experiments

4.1 Experimental Settings

Training Details. Our training data are sampled from FoundIR [25] and RealCE [32]. Progressive training sequences are constructed as described in Sec. 3.2 to facilitate gradual restoration learning. Unless otherwise specified, we randomly select 50 samples per task category from each dataset (FoundIR and RealCE) for training, and also use 50 samples per category for the drift correction stage. Both models adopt Wan2.2-TI2V-5B [39] as the backbone network. More implementation and training details are provided in Appendix A.1.

Test Details. We evaluate our method on the FoundIR [25] test split, covering diverse degradations including blur, noise, JPEG compression, haze, rain, rain-drop, low-light conditions, and mixed degradations. In addition, we report results on several external benchmark datasets [1, 2, 6, 9, 16, 40] to further validate cross-dataset generalization and real-world applicability. We further evaluate out-of-distribution (OOD) robustness in Sec. 4.4 to examine model stability under unseen and more severe degradation scenarios. These evaluations are designed to comprehensively verify both restoration quality and generalization capability. More implementation and evaluation details are provided in Appendix A.2.

Evaluation Metrics. We evaluate restoration quality using PSNR and SSIM, two widely adopted metrics in image restoration. PSNR quantifies pixel-wise reconstruction fidelity, while SSIM measures structural consistency between the restored image and the ground truth. Higher values for both metrics indicate better performance. Details are provided in the Appendix A.2.

Table 1: Quantitative comparison ($\frac{\text{PSNR}}{\text{SSIM}}$, both higher is better) on the FoundIR test set. FoundIR-G denotes the generalist model of FoundIR and DC denotes Drift Correction. Underlining and boldface denote the second-best and best methods, respectively.

	Real-ESRGAN	DGUNet	Trans-Weather	PromptIR	DiffUIR	DA-CLIP	X-Restormer	InstructIR	AutoDIR	FoundIR-G	Ours w/o DC	Ours
Data Scale	15K	16K	19K	77K	30K	53K	40K	15K	23K	1M	1K	1K
Blur	<u>25.20</u> <u>0.7868</u>	21.86 0.7334	21.34 0.7103	21.91 0.7339	25.31 0.7979	20.92 0.6954	21.88 0.7325	20.15 0.6801	20.31 0.6946	24.34 0.7856	21.02 0.6862	24.92 0.7809
Noise	34.46 0.9585	36.69 0.9494	30.12 0.8945	36.57 0.9478	34.48 0.9622	29.45 0.9027	35.86 0.9412	<u>38.58</u> <u>0.9628</u>	36.84 0.9221	38.61 0.9662	32.61 0.9397	32.87 0.9498
JPEG	27.62 0.9108	29.80 0.8906	23.52 0.7296	29.63 0.8842	30.09 0.9390	25.77 0.7816	28.58 0.8646	<u>32.99</u> 0.9378	32.77 0.9280	34.03 0.9379	28.21 0.8487	26.59 0.8269
Haze	22.07 0.8380	18.58 0.6762	17.72 0.5635	15.36 0.4982	19.97 <u>0.8193</u>	15.91 0.5399	16.47 0.6257	16.85 0.7555	15.23 0.6264	16.65 0.7814	21.25 0.6918	<u>21.70</u> 0.6711
Rain	28.95 0.9226	25.47 0.8245	23.49 0.6886	27.59 0.8411	30.17 <u>0.9350</u>	23.04 0.6849	25.70 0.8076	<u>30.18</u> 0.8997	25.69 0.7711	33.09 0.9387	26.40 0.7957	25.42 0.7836
Raindrop	28.94 0.9115	24.83 0.7924	22.94 0.6814	25.83 0.8327	26.98 0.8908	20.86 0.6490	26.11 0.8368	21.05 0.6828	20.82 0.6687	<u>28.52</u> <u>0.9110</u>	25.77 0.7698	24.99 0.7380
Lowlight	19.26 <u>0.8709</u>	16.16 0.6494	14.95 0.6295	16.33 0.6353	14.02 0.7101	17.34 0.7412	16.02 0.6404	20.04 0.8542	<u>21.90</u> 0.8288	12.35 0.7185	19.18 0.8278	26.94 0.8944
B+N	23.48 0.7728	22.90 0.7633	22.19 0.7363	22.93 0.7587	<u>24.44</u> <u>0.8039</u>	22.15 0.7293	22.90 0.7544	21.70 0.7185	21.90 0.7293	22.53 0.7654	23.80 0.7703	27.31 0.8471
B+J	20.41 0.6562	22.86 0.7358	22.14 0.7105	22.90 0.7360	21.36 0.6915	21.36 0.6940	22.85 0.7321	21.39 0.6814	22.03 0.7088	28.33 0.8491	24.05 0.7571	<u>25.33</u> <u>0.8020</u>
N+J	29.71 0.9566	35.28 0.9564	25.59 0.8377	35.08 0.9524	31.96 0.9782	26.03 0.8602	33.83 0.9405	39.90 <u>0.9770</u>	37.55 0.9616	<u>39.21</u> 0.9745	33.33 0.9422	31.63 0.9323
R+H	20.40 <u>0.7153</u>	18.79 0.4981	18.43 0.4245	16.61 0.4985	<u>20.24</u> 0.7268	13.97 0.3563	15.17 0.4354	13.49 0.5535	14.90 0.4213	15.42 0.6766	18.70 0.5574	18.69 0.5222
L+H	21.79 0.8084	13.20 0.4182	15.99 0.4285	15.36 0.4982	19.31 0.7745	12.62 0.3220	14.75 0.4416	13.52 0.4983	14.50 0.4456	17.05 0.7556	19.74 0.5983	<u>20.79</u> <u>0.6209</u>
L+R	32.16 0.9116	30.66 0.9097	28.29 0.8663	31.03 0.9039	32.35 <u>0.9255</u>	21.58 0.7246	30.93 0.9026	29.87 0.8866	27.15 0.8576	<u>32.77</u> 0.9281	32.90 0.9126	31.27 0.9064
L+B	<u>21.95</u> 0.7254	11.54 0.4922	21.35 0.6764	20.29 0.6723	18.97 0.6939	16.17 0.6241	19.38 0.6605	17.43 0.6676	19.14 0.6570	18.07 0.7551	20.37 0.6543	23.78 <u>0.7378</u>
L+N	17.49 0.7358	12.56 0.5349	11.56 0.5181	10.83 0.4499	13.88 0.6262	15.70 0.6365	9.75 0.3866	16.37 0.4625	<u>17.49</u> 0.6900	12.77 <u>0.7454</u>	17.36 0.6842	24.60 0.7765
L+J	22.89 <u>0.8704</u>	12.17 0.5433	19.16 0.6528	21.52 0.7671	19.98 0.8706	15.86 0.6048	18.66 0.7205	18.06 0.7787	16.14 0.6375	17.66 0.8489	<u>22.72</u> 0.7635	22.89 0.7400
L+B+N	21.43 0.6612	10.60 0.4608	20.83 0.6607	22.63 <u>0.6924</u>	18.89 0.6705	15.30 0.6202	<u>22.00</u> 0.6841	12.78 0.5392	18.91 0.6499	17.63 0.6889	20.41 0.6362	24.20 0.7491
L+B+J	19.49 0.6582	9.57 0.4897	19.64 0.6918	12.40 0.5597	18.64 0.6751	12.46 0.5774	13.63 0.5738	17.39 0.7092	16.91 0.6761	18.64 <u>0.7899</u>	<u>21.16</u> 0.7514	25.71 0.8094
L+N+J	<u>26.11</u> 0.9496	9.64 0.5456	21.41 0.8068	22.71 0.8616	20.66 <u>0.9338</u>	15.34 0.7068	16.40 0.7810	19.13 0.9105	18.78 0.8122	20.09 0.9162	26.09 0.9115	27.64 0.9161
B+N+J	21.40 0.7197	22.43 0.6945	21.64 0.6577	22.47 0.6942	0.7861 0.6589	21.19 0.6589	22.41 0.6894	22.42 0.6980	22.37 0.6876	26.72 0.7310	24.69 0.7659	<u>25.46</u> <u>0.7787</u>
Average	<u>24.26</u> <u>0.8173</u>	20.27 0.6779	21.11 0.6782	22.49 0.7209	23.27 0.8105	19.15 0.6554	21.66 0.7075	22.18 0.7426	22.07 0.7187	23.57 0.8199	23.68 0.7490	25.18 0.7729

4.2 Comparative Experiment

We first evaluate our method on the FoundIR test set, as shown in Tab. 1, comparing with restoration methods including Real-ESRGAN [41], DGUNet [34], TransWeather [38], PromptIR [36], DiffUIR [46], DA-CLIP [31], X-Restormer [10], InstructIR [11], AutoDIR [20], FoundIR [25]. Since we develop an all-in-one image restoration model, we compare with FoundIR-Generalist (FoundIR-G), its all-in-one variant. **Trained with only 1K samples from the FoundIR training set, which accounts for merely 0.1% to 7% of the data used by existing approaches, our method matches or surpasses prior methods on the FoundIR test set.** Notably, compared with FoundIR models trained on 1M samples, our method even outperforms the all-in-one variant (FoundIR-G) of FoundIR trained using 1M samples on several metrics. The qualitative results

Table 2: Quantitative comparisons ($\frac{\text{PSNR}}{\text{SSIM}}$) on the public benchmarks. Underlining and boldface indicate the second-best and best methods, respectively.

Methods		PromptIR	TransWeather	DA-CLIP	DiffUIR	AutoDIR	InstructIR	X-Restormer	AgenticIR	FoundIR-G	Ours
Data Scale ↓		77K	19K	53K	30K	23K	80K	40K	15K	1M	1K
Dense-Haze	PSNR ↑	9.57	10.51	10.94	9.59	12.33	11.03	9.57	10.11	9.29	<u>11.97</u>
	SSIM ↑	0.4333	0.4523	0.459	0.4326	<u>0.4862</u>	0.4649	0.4295	0.3884	0.4307	0.4897
UHD-LL	PSNR ↑	11.76	12.3	18.51	11.27	22.52	<u>20.03</u>	11.56	12.82	10.61	17.87
	SSIM ↑	0.6170	0.6557	<u>0.8120</u>	0.5975	0.8572	0.7356	0.6113	0.6649	0.5775	0.7999
NH-Haze	PSNR ↑	11.38	11.58	12.35	11.39	<u>12.71</u>	12.24	11.36	12.2	11.43	12.97
	SSIM ↑	0.4343	0.4110	0.4662	0.422	<u>0.4774</u>	0.4984	0.4131	0.4495	0.4491	0.4241
UAV-Rain1k	PSNR ↑	15.16	14.85	15.38	15.2	<u>15.41</u>	13.75	15.16	14.26	15.11	15.56
	SSIM ↑	0.6605	0.5381	0.6035	0.6389	0.5834	0.3240	0.6397	0.5300	<u>0.6411</u>	0.5152
HQ-NightRain	PSNR ↑	10.43	12.88	14.78	11.58	11.67	10.92	10.33	<u>16.29</u>	11.57	27.70
	SSIM ↑	0.4485	0.4774	0.5398	0.4827	0.4697	0.3972	0.4376	<u>0.5681</u>	0.5220	0.8747

in Fig. 3 further confirm its superiority. These results demonstrate remarkable data efficiency and clearly validate the effectiveness of introducing pretrained video generative priors, which substantially enhance restoration capability under severely constrained training data.

More importantly, the superiority of our method extends beyond in domain evaluation. Results on out of distribution benchmarks including Dense-Haze [1], UHD-LL [40], NH-Haze [2], UAV-Rain1K [6], and HQ-NightRain [9], as shown in Tab. 2, demonstrate strong cross dataset generalization, where our method consistently achieves clear performance gains over competing approaches. This further confirms that video generative models implicitly capture robust and transferable visual priors, which can be effectively adapted to restoration scenarios.

We also evaluate the effectiveness of our correction module. As reported in Tab. 1, PSNR increases by 1.4 dB and SSIM improves by 0.024. Visual comparisons in Fig. 5(a) also demonstrate enhanced perceptual fidelity. We attribute these gains to the resolution bias of video generative models, where models are typically trained on moderate resolution data such as 720p [39], which limits the ability to recover high frequency textures. By incorporating a dedicated correction model for detail enhancement, our method decouples structural restoration from high frequency recovery, leading to improved reconstruction quality.

We also show qualitative comparisons of the video generative model before and after fine tuning in Fig.4. The off the shelf model struggles to understand the restoration task, which demonstrates the necessity of our few shot training strategy. Our approach effectively unlocks the task specific potential of pretrained generative priors, enabling high fidelity restoration with strong data efficiency.

These results provide strong evidence that video generative models can serve as general visual foundation models for low-

**Fig. 4:** Performance improvement on the test dataset of FoundIR brought by few-shot training.

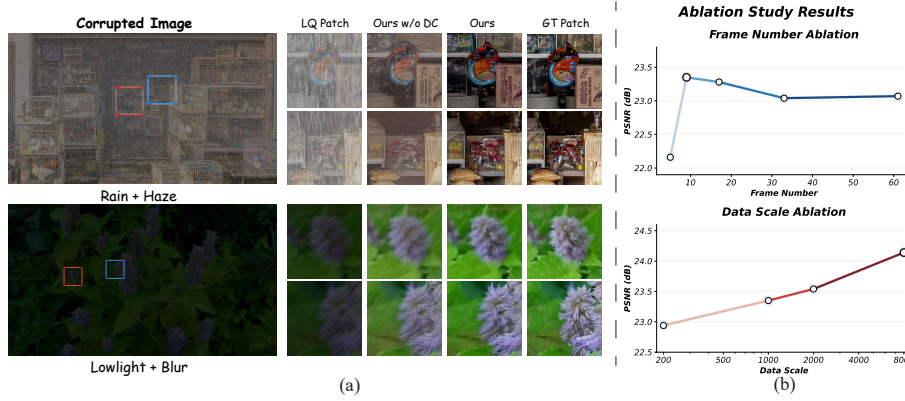


Fig. 5: (a) Comparison on the FoundIR test set with and without the refine model. GT denotes ground truth. Correction improves visual quality and enhances fine details. (b) Ablation study results. Top: effect of different training frame numbers for image restoration. Bottom: performance improves as training data scale increases.

Table 3: Ablation study about the number of frames ($\frac{\text{PSNR}}{\text{SSIM}}$, both higher is better).

Methods	Isolated Degradation								Coupled Degradation												Average
	Blur	Noise	JPEG	Haze	Rain	Raindrop	Lowlight		B+N	B+J	N+J	R+H	L+H	L+R	L+B	L+N	L+J	L+B+N	L+B+J	L+N+J	
5 frames	21.25	31.20	26.49	17.20	25.01	<u>25.29</u>	19.55	25.11	24.50	27.07	14.39	18.15	30.76	19.92	15.22	21.17	20.33	21.11	22.80	24.73	22.16
	0.6852	0.9439	<u>0.8258</u>	0.6119	<u>0.7697</u>	0.7524	0.8477	0.8012	0.7551	0.8668	0.4491	<u>0.5811</u>	0.8933	<u>0.6515</u>	0.6256	0.7214	<u>0.6510</u>	0.7385	0.8971	<u>0.7525</u>	0.7242
9 frames	21.42	33.60	27.05	20.32	<u>25.54</u>	25.62	20.62	23.34	23.09	26.39	18.18	19.70	32.64	21.24	16.93	22.72	23.12	<u>22.37</u>	25.52	21.54	23.35
	<u>0.7923</u>	<u>0.9404</u>	0.8294	<u>0.6833</u>	0.7615	<u>0.7516</u>	0.8405	0.7550	0.7181	0.8541	<u>0.5330</u>	0.5923	0.9069	0.6564	0.6879	0.7594	0.7115	0.7466	<u>0.8916</u>	0.6770	0.7385
17 frames	22.05	<u>33.86</u>	26.32	21.32	24.69	24.51	<u>20.08</u>	24.41	24.26	28.36	<u>18.45</u>	19.23	32.20	19.78	16.53	<u>21.62</u>	<u>20.36</u>	23.03	<u>24.29</u>	22.93	<u>23.28</u>
	0.7100	0.9353	0.8166	0.6849	0.7439	0.7359	<u>0.8455</u>	0.7790	<u>0.7732</u>	0.8964	0.5338	0.5767	0.8976	0.6302	<u>0.6880</u>	<u>0.7387</u>	0.6337	0.7851	0.8977	0.7111	<u>0.7370</u>
33 frames	20.65	34.04	26.12	20.60	24.86	24.52	19.99	23.14	26.27	<u>20.51</u>	18.15	19.18	<u>32.30</u>	18.98	<u>16.86</u>	21.31	19.66	20.81	24.11	25.59	23.04
	0.6808	0.9295	0.8006	0.6665	0.7473	0.7228	0.8434	0.7483	0.7937	<u>0.9025</u>	0.5204	0.5640	<u>0.9034</u>	0.6378	0.6896	0.7298	0.6248	<u>0.7571</u>	0.8939	0.7640	0.7294
61 frames	<u>21.62</u>	33.60	25.87	<u>20.65</u>	26.25	24.90	19.33	<u>24.49</u>	24.12	31.00	19.29	<u>19.42</u>	31.77	<u>20.25</u>	12.43	19.70	20.01	21.63	23.16	23.04	23.07
	0.6889	0.9360	0.7971	0.6457	0.7842	0.7253	0.8024	<u>0.7807</u>	0.7489	0.9164	0.5300	0.5721	0.8996	0.6091	0.5589	0.7064	0.6181	0.7326	0.8800	0.7213	0.7199

level vision tasks. By formulating restoration as a progressive generative refinement process, our approach demonstrates that high-quality restoration capability can be efficiently activated under few-shot supervision. This suggests a scalable paradigm toward universal visual prior learning, enabling effective knowledge transfer across diverse degradation types and low-level vision tasks in practice.

4.3 Ablation Study

Frame Count. We analyze the impact of frame numbers in the video generation process for image restoration. As shown in Tab.3 and Fig.5(b), we evaluate frame numbers ranging from 5 to 61 on the FoundIR test set. Interestingly, performance does not monotonically improve with more frames. Instead, the 9-frame setting consistently yields better results than 33 and 61 frames.

This observation suggests that the generative prior learned by the video model primarily emphasizes global structural coherence rather than fine grained temporal modeling. In this view, image restoration can be formulated as a conditional generative process guided by strong semantic and geometric priors, where missing content is inferred through high level structural reasoning. Therefore,

Table 4: Ablation study on Progressive Curriculum Training ($\frac{\text{PSNR}}{\text{SSIM}}$).

Resolution	Isolated Degradation							Coupled Degradation													Average
	Blur	Noise	JPEG	Haze	Rain	Raindrop	Lowlight	B+N	B+J	N+J	R+H	L+H	L+R	L+B	L+N	L+J	L+B+N	L+B+J	L+N+J	B+N+J	
512	21.25	31.20	26.49	17.20	25.01	25.29	19.55	25.11	24.50	27.07	14.39	18.15	30.76	19.92	15.22	21.17	20.33	21.11	22.80	<u>24.73</u>	22.16
	0.6852	0.9439	0.8258	0.6119	0.7697	0.7524	<u>0.8477</u>	0.8012	0.7551	0.8668	0.4491	0.5811	0.8933	<u>0.6515</u>	0.6256	0.7214	0.6510	0.7385	0.8971	<u>0.7525</u>	0.7242
720	22.33	<u>33.64</u>	27.97	20.64	25.76	25.63	19.34	22.24	23.21	28.48	19.79	<u>19.57</u>	32.06	19.18	<u>17.26</u>	22.63	<u>22.10</u>	21.95	24.83	21.45	23.35
	0.7253	<u>0.9460</u>	0.8464	0.6854	0.7792	0.7623	0.8363	0.7275	0.7131	0.8869	0.5594	<u>0.5948</u>	0.9010	0.6411	0.7036	0.7631	0.7030	0.7368	0.9055	0.6823	0.7442
960	21.55	34.40	28.10	20.55	<u>26.37</u>	25.47	19.45	23.42	25.87	33.60	<u>18.73</u>	18.01	32.18	18.81	17.18	22.25	19.50	20.48	<u>25.82</u>	22.85	23.41
	<u>0.7089</u>	0.9454	<u>0.8477</u>	<u>0.6867</u>	0.7970	0.7700	0.8294	0.7657	0.7937	0.9440	0.5570	0.5808	<u>0.9112</u>	0.6404	0.6782	0.7555	0.6312	0.7402	0.9097	0.7167	0.7474
512+720	<u>21.70</u>	30.71	<u>28.18</u>	<u>21.08</u>	25.76	25.93	<u>19.89</u>	<u>24.29</u>	25.55	28.99	18.61	19.13	<u>32.71</u>	20.83	17.62	<u>22.65</u>	22.45	23.86	25.59	23.11	<u>23.59</u>
	0.6999	0.9394	<u>0.8469</u>	0.6842	0.7693	0.7640	0.8256	0.7718	0.7900	0.8876	0.5377	0.5862	0.9103	0.6438	0.6840	0.7687	<u>0.6852</u>	0.7832	<u>0.9101</u>	0.7117	<u>0.7451</u>
720+512	21.38	32.32	26.87	19.43	25.36	25.40	19.95	24.15	<u>23.78</u>	26.40	16.01	18.74	31.96	20.03	17.23	22.03	20.26	<u>22.10</u>	23.85	24.77	22.90
	0.6951	0.9416	0.8341	0.6612	0.7683	0.7596	0.8394	<u>0.7730</u>	<u>0.7730</u>	0.8572	0.4952	0.5742	0.9024	0.6430	0.6915	0.7512	0.6198	<u>0.7637</u>	0.9011	<u>0.7541</u>	0.7355
512+720+960	21.02	32.61	28.21	21.25	26.40	<u>25.77</u>	19.18	23.80	24.05	<u>33.33</u>	18.70	19.74	32.90	<u>20.37</u>	<u>17.36</u>	22.72	20.41	21.16	26.09	24.69	23.68
	0.6862	0.9397	0.8487	0.6918	<u>0.7957</u>	<u>0.7698</u>	0.8278	0.7703	0.7571	<u>0.9422</u>	<u>0.5574</u>	0.5983	0.9126	0.6543	0.6842	<u>0.7635</u>	0.6362	0.7514	0.9115	0.7659	0.7490

increasing the number of frames does not necessarily provide additional informative signals, as neighboring frames tend to become semantically redundant under smooth restoration trajectories in the latent space. Consequently, a moderate number of frames is sufficient for approximating the restoration process, while excessive temporal sampling may introduce redundant constraints and increase computational burden without significant performance gains. This further indicates that restoration performance is mainly determined by learned spatial semantic priors rather than dense temporal sampling.

Progressive Curriculum Training. We study the effectiveness of the proposed progressive curriculum training strategy, as shown in Tab. 4, where we compare fixed resolution training with different progressive schedules. Here, numbers denote the training resolution (e.g., 512 indicates resizing the input image such that the shorter side is aligned to 512 while preserving the aspect ratio, followed by 512×512 random cropping). All models are trained for 300 epochs in total, with epochs evenly distributed across stages for multi-stage training.

The results show that performance consistently improves with increasing resolution, since higher resolutions provide richer high frequency structural and textural cues for learning more discriminative restoration priors. Moreover, progressive resolution training outperforms single resolution training (e.g., 512+720 and 512+720+960), suggesting that a coarse to fine optimization paradigm better matches the hierarchical nature of image restoration. In contrast, decreasing resolution schedules lead to performance degradation (e.g. 720+512), as the model tends to prioritize global appearance consistency while sacrificing fine detail modeling. Overall, the proposed strategy consistently enhances both training stability and restoration quality by better aligning optimization with the intrinsic coarse to fine restoration process.

4.4 Discussions

Few-shot Capability. We discuss the effectiveness of leveraging video generation priors for few shot image restoration. As shown in Tab. 1, our method achieves competitive or even superior performance while using significantly less training data. Specifically, our model is trained using only 0.1% – 7% of the data required by conventional methods, demonstrating that large scale video generative pretraining captures strong generic structural and motion aware priors that

Table 5: Ablation study about the scale of training data ($\frac{\text{PSNR}}{\text{SSIM}}$, both higher is better).

Data Scale	Isolated Degradation							Coupled Degradation											Average		
	Bhr	Noise	JPEG	Haze	Rain	Raindrop	Lowlight	B+N	B+J	N+J	R+H	L+H	L+R	L+B	L+N	L+J	L+B+N	L+B+J		L+N+J	B+N+J
0.2K	22.14	33.90	27.01	19.64	25.96	24.34	20.21	22.49	22.03	<u>30.06</u>	18.64	18.52	30.37	21.39	<u>16.85</u>	19.41	21.85	20.37	23.91	21.85	22.94
	0.7213	0.9463	0.8340	0.6568	0.7964	0.7540	0.8548	0.7380	0.6789	0.9156	0.5297	0.5822	0.8931	0.6811	0.6414	0.7064	<u>0.7109</u>	0.6582	0.9116	<u>0.6954</u>	0.7390
1K	<u>22.33</u>	<u>33.64</u>	27.97	<u>20.64</u>	25.76	<u>25.63</u>	19.34	22.24	23.21	28.48	<u>19.79</u>	19.57	<u>32.06</u>	19.18	17.36	22.63	<u>22.10</u>	21.95	24.83	21.45	23.35
	<u>0.7253</u>	0.9440	0.8464	0.6854	0.7792	0.7623	0.8363	0.7275	0.7131	0.8869	0.5594	0.5948	0.9010	0.6411	0.7036	0.7631	0.7030	0.7368	0.9055	0.6823	0.7442
2K	21.92	31.98	27.50	19.64	26.73	25.74	<u>20.63</u>	25.79	<u>25.18</u>	28.86	18.37	<u>19.81</u>	32.25	<u>21.63</u>	16.08	<u>22.26</u>	22.08	21.01	<u>26.28</u>	<u>23.79</u>	<u>23.54</u>
	0.7082	0.9432	0.8361	0.6501	0.8003	<u>0.7611</u>	0.8630	0.8199	<u>0.7718</u>	0.8930	0.5273	<u>0.6120</u>	0.9081	<u>0.6822</u>	<u>0.6486</u>	<u>0.7367</u>	0.6946	<u>0.7447</u>	<u>0.9135</u>	0.7279	<u>0.7469</u>
8K	22.98	33.41	<u>27.57</u>	<u>21.18</u>	<u>26.54</u>	25.11	21.49	<u>25.10</u>	26.02	30.64	19.97	20.00	31.67	21.76	16.28	21.14	22.86	<u>21.86</u>	28.27	23.91	24.14
	0.7284	<u>0.9454</u>	<u>0.8375</u>	<u>0.6704</u>	<u>0.7982</u>	<u>0.7611</u>	<u>0.8628</u>	<u>0.7999</u>	0.7827	<u>0.9088</u>	<u>0.5562</u>	0.6200	<u>0.9063</u>	0.7153	0.6458	0.7214	0.7354	0.7505	0.9137	0.6786	0.7549

Table 6: Quantitative comparisons ($\frac{\text{PSNR}}{\text{SSIM}}$) on the unseen task for our method about desnowing. Underlining and boldface indicate the second-best and best methods, respectively. FoundIR-G denotes the generalist version of FoundIR.

Methods	PromptIR	TransWeather	DA-CLIP	DiffUIR	X-Restormer	AgenticIR	FoundIR-G	Ours
Data Scale ↓	77K	19K	53K	30K	40K	<u>15K</u>	1M	1K
WeatherBench	PSNR ↑	21.54	20.94	<u>21.59</u>	21.68	21.57	20.35	21.57
	SSIM ↑	0.7767	0.7579	0.7731	<u>0.7795</u>	0.7813	0.7304	0.7794

can be transferred to restoration tasks. From a learning perspective, our approach focuses on activating and adapting pretrained generative knowledge with limited task specific image restoration supervision, reducing data dependency while preserving model expressiveness.

As shown in Tab.5 and Fig.5, the performance of our method consistently improves as the amount of training data increases. For a fair comparison, all models are trained for 300 epochs at a fixed 720 resolution. Notably, using only 200 training samples, our method already achieves performance comparable to existing full-data baselines, highlighting strong data efficiency and generalization capability. This suggests that the pretrained video generative prior acts as a powerful regularization mechanism, enabling robust restoration under limited supervision while allowing further performance gains as more data becomes available. However, it is worth noting that expanding the training set does not consistently improve performance across all degradation types, suggesting a potential trade-off or balance during model learning.

Overall, these results further validate the strong potential of exploiting video generative priors for few-shot image restoration, suggesting that large-scale generative pretraining can serve as a general knowledge foundation for data-efficient visual learning. By transferring high-level semantic, structural, and motion-aware priors from video, generative models provide a promising paradigm for building scalable and data-efficient visual intelligence that generalizes beyond restoration tasks to broader visual understanding and synthesis problems.

Generalization Capability. As shown in Tab. 2, although trained on only a 1K subset of FoundIR training data, our model generalizes well to multiple external benchmarks and achieves performance comparable to top-tier methods, demonstrating strong data efficiency and the feasibility of competitive restoration without large scale task specific supervision.

Furthermore, Fig. 6 and Tab. 6 present qualitative and quantitative results on snow removal [16], an unseen task for our model. Although trained with only lim-

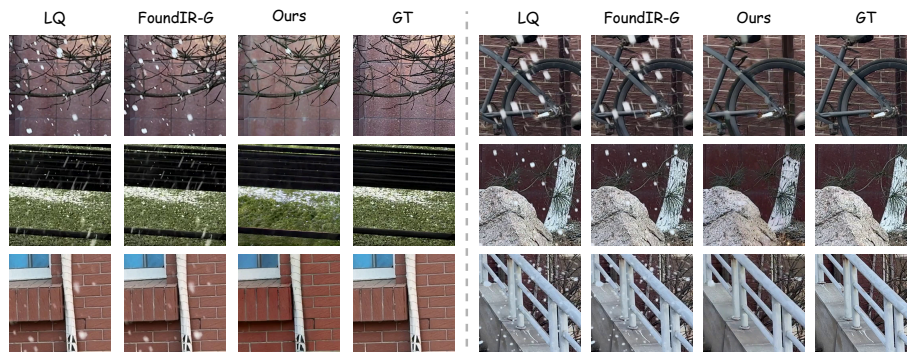


Fig. 6: Visualization results on an OOD snow removal scenario. FoundIR-G denotes the Generalist model of FoundIR. GT denotes ground truth. Both methods are evaluated under OOD conditions. Although our model is trained with only 1K samples, it shows significantly better generalization than FoundIR-G trained with 1M images.

ited image restoration data and without additional training on new degradation types, the model generalizes effectively to unseen corruptions and successfully removes snow artifacts while producing visually coherent and competitive results. This demonstrates that the model can learn transferable restoration priors and directly transfer knowledge learned during pretraining to new tasks, such as applying its understanding of snow patterns to desnowing tasks. This capability reflects the strong inductive power of video generation models, which can implicitly capture rich semantic and structural knowledge during pretraining. It is particularly important for few-shot image restoration, where minimal training data is sufficient to enable universal degradation modeling. Overall, these results highlight the strong generalization potential of generative foundation models, showing that minimal supervision can unlock broad cross-domain adaptability and pave the way toward more general visual intelligence.

5 Conclusion

In this paper, we introduced V-Bridge, a framework that unlocks the restoration capability of pretrained video generative models with few-shot training. By reformulating restoration as a progressive generative refinement process and exploiting chain-like frame reasoning, we show that video foundation models can serve as powerful and transferable visual priors. Remarkably, our approach activates strong restoration capability using only a very small number of task-specific samples, further demonstrating the broad potential of video generative models beyond video synthesis. We also propose efficient progressive resolution training and lightweight refinement strategies to achieve high-fidelity restoration under limited supervision. This work provides new evidence that video generative models can serve as general visual foundation models and opens new directions for unified generative modeling in vision tasks.

References

1. Ancuti, C.O., Ancuti, C., Sbert, M., Timofte, R.: Dense-haze: A benchmark for image dehazing with dense-haze and haze-free images. In: 2019 IEEE international conference on image processing (ICIP). pp. 1014–1018. IEEE (2019)
2. Ancuti, C.O., Ancuti, C., Timofte, R.: NH-HAZE: an image dehazing benchmark with non-homogeneous hazy and haze-free images. In: Proceedings of the IEEE Conference on Computer Vision and Pattern Recognition Workshops. IEEE CVPR 2020 (2020)
3. Banham, M.R., Katsaggelos, A.K.: Digital image restoration. IEEE signal processing magazine **14**(2), 24–41 (2002)
4. Blattmann, A., Dockhorn, T., Kulal, S., Mendelvitich, D., Kilian, M., Lorenz, D., Levi, Y., English, Z., Voleti, V., Letts, A., et al.: Stable video diffusion: Scaling latent video diffusion models to large datasets. arXiv preprint arXiv:2311.15127 (2023)
5. Brooks, T., Peebles, B., Holmes, C., DePue, W., Guo, Y., Jing, L., Schnurr, D., Taylor, J., Luhman, T., Luhman, E., Ng, C., Wang, R., Ramesh, A.: Video generation models as world simulators (2024), <https://openai.com/research/video-generation-models-as-world-simulators>
6. Chang, W., Chen, H., He, X., Chen, X., Shen, L.: Uav-rain1k: A benchmark for raindrop removal from uav aerial imagery. In: Proceedings of the IEEE/CVF Conference on Computer Vision and Pattern Recognition. pp. 15–22 (2024)
7. Chen, H., Xia, M., He, Y., Zhang, Y., Cun, X., Yang, S., Xing, J., Liu, Y., Chen, Q., Wang, X., et al.: Videocrafter1: Open diffusion models for high-quality video generation. arXiv preprint arXiv:2310.19512 (2023)
8. Chen, H.H., Lan, D., Shu, W.J., Liu, Q., Wang, Z., Chen, S., Cheng, W., Chen, K., Zhang, H., Zhang, Z., et al.: Tivibench: Benchmarking think-in-video reasoning for video generative models. arXiv preprint arXiv:2511.13704 (2025)
9. Chen, X., Pan, J., Dong, J., Tang, J.: Towards unified deep image deraining: A survey and a new benchmark. IEEE Transactions on Pattern Analysis and Machine Intelligence (2025)
10. Chen, X., Li, Z., Pu, Y., Liu, Y., Zhou, J., Qiao, Y., Dong, C.: A comparative study of image restoration networks for general backbone network design. In: European Conference on Computer Vision. pp. 74–91. Springer (2024)
11. Conde, M.V., Geigle, G., Timofte, R.: Instructir: High-quality image restoration following human instructions. In: Proceedings of the European Conference on Computer Vision (ECCV) (2024)
12. Deng, H.: Video models start to solve chess, maze, sudoku, mental rotation, and raven matrices. arXiv preprint arXiv:2512.05969 (2025)
13. Fang, Y., Zhang, H., Wong, H.S., Zeng, T.: A robust non-blind deblurring method using deep denoiser prior. In: Proceedings of the IEEE/CVF conference on computer vision and pattern recognition. pp. 735–744 (2022)
14. Gao, Y., Guo, H., Hoang, T., Huang, W., Jiang, L., Kong, F., Li, H., Li, J., Li, L., Li, X., et al.: Seedance 1.0: Exploring the boundaries of video generation models. arXiv preprint arXiv:2506.09113 (2025)
15. Google DeepMind: Veo (2025), <https://deepmind.google/models/veo>
16. Guan, Q., Yang, Q., Chen, X., Song, T., Jin, G., Jin, J.: Weatherbench: A real-world benchmark dataset for all-in-one adverse weather image restoration. In: Proceedings of the 33rd ACM international conference on multimedia. pp. 12607–12613 (2025)

17. Guo, C.L., Yan, Q., Anwar, S., Cong, R., Ren, W., Li, C.: Image dehazing transformer with transmission-aware 3d position embedding. In: Proceedings of the IEEE/CVF conference on computer vision and pattern recognition. pp. 5812–5820 (2022)
18. Guo, Z., Chen, X., Zhang, R., An, R., Qi, Y., Jiang, D., Li, X., Zhang, M., Li, H., Heng, P.A.: Are video models ready as zero-shot reasoners? an empirical study with the mme-cof benchmark. arXiv preprint arXiv:2510.26802 (2025)
19. Ho, J., Chan, W., Saharia, C., Whang, J., Gao, R., Gritsenko, A., Kingma, D.P., Poole, B., Norouzi, M., Fleet, D.J., et al.: Imagen video: High definition video generation with diffusion models. arXiv preprint arXiv:2210.02303 (2022)
20. Jiang, Y., Zhang, Z., Xue, T., Gu, J.: Autodir: Automatic all-in-one image restoration with latent diffusion. In: European Conference on Computer Vision. pp. 340–359. Springer (2024)
21. Jin, X., Han, L.H., Li, Z., Guo, C.L., Chai, Z., Li, C.: Dnf: Decouple and feedback network for seeing in the dark. In: Proceedings of the IEEE/CVF conference on computer vision and pattern recognition. pp. 18135–18144 (2023)
22. Kong, W., Tian, Q., Zhang, Z., Min, R., Dai, Z., Zhou, J., Xiong, J., Li, X., Wu, B., Zhang, J., et al.: Hunyuanvideo: A systematic framework for large video generative models. arXiv preprint arXiv:2412.03603 (2024)
23. Kuaishou: Kling video model. <https://kling.kuaishou.com/en> (2024)
24. Li, B., Liu, X., Hu, P., Wu, Z., Lv, J., Peng, X.: All-In-One Image Restoration for Unknown Corruption. In: IEEE Conference on Computer Vision and Pattern Recognition. New Orleans, LA (Jun 2022)
25. Li, H., Chen, X., Dong, J., Tang, J., Pan, J.: Foundir: Unleashing million-scale training data to advance foundation models for image restoration. In: Proceedings of the IEEE/CVF international conference on computer vision. pp. 12626–12636 (2025)
26. Li, Y., Gu, Y., Min, Y., Liu, Z., Du, Y., Zhou, K., Yang, M., Zhao, W.X., Qiu, M.: Viper: Process-aware evaluation for generative video reasoning. arXiv preprint arXiv:2512.24952 (2025)
27. Liang, J., Cao, J., Sun, G., Zhang, K., Van Gool, L., Timofte, R.: Swinir: Image restoration using swin transformer. In: Proceedings of the IEEE/CVF international conference on computer vision. pp. 1833–1844 (2021)
28. Liang, J., Cao, J., Sun, G., Zhang, K., Van Gool, L., Timofte, R.: Swinir: Image restoration using swin transformer. In: Proceedings of the IEEE/CVF international conference on computer vision. pp. 1833–1844 (2021)
29. Lin, X., He, J., Chen, Z., Lyu, Z., Dai, B., Yu, F., Qiao, Y., Ouyang, W., Dong, C.: Diffbir: Toward blind image restoration with generative diffusion prior. In: European conference on computer vision. pp. 430–448. Springer (2024)
30. Luo, Y., Zhao, X., Lin, B., Zhu, L., Tang, L., Liu, Y., Chen, Y.C., Qian, S., Wang, X., You, Y.: V-reasonbench: Toward unified reasoning benchmark suite for video generation models. arXiv preprint arXiv:2511.16668 (2025)
31. Luo, Z., Gustafsson, F.K., Zhao, Z., Sjölund, J., Schön, T.B.: Controlling vision-language models for multi-task image restoration. In: The Twelfth International Conference on Learning Representations (2024), <https://openreview.net/forum?id=t3vnnLeajU>
32. Ma, J., Liang, Z., Xiang, W., Yang, X., Zhang, L.: A benchmark for chinese-english scene text image super-resolution. In: Proceedings of the IEEE/CVF international conference on computer vision. pp. 19452–19461 (2023)

33. Ma, J., Cheng, T., Wang, G., Zhang, Q., Wang, X., Zhang, L.: Prores: Exploring degradation-aware visual prompt for universal image restoration. arXiv preprint arXiv:2306.13653 (2023)
34. Mou, C., Wang, Q., Zhang, J.: Deep generalized unfolding networks for image restoration. In: Proceedings of the IEEE/CVF conference on computer vision and pattern recognition. pp. 17399–17410 (2022)
35. Peebles, W., Xie, S.: Scalable diffusion models with transformers. In: Proceedings of the IEEE/CVF international conference on computer vision. pp. 4195–4205 (2023)
36. Potlapalli, V., Zamir, S.W., Khan, S.H., Shahbaz Khan, F.: Promptir: Prompting for all-in-one image restoration. *Advances in neural information processing systems* **36**, 71275–71293 (2023)
37. Tong, C., Chang, M., Zhang, S., Wang, Y., Liang, C., Zhao, Z., An, R., Zeng, B., Shi, Y., Dai, Y., et al.: Cof-t2i: Video models as pure visual reasoners for text-to-image generation. arXiv preprint arXiv:2601.10061 (2026)
38. Valanarasu, J.M.J., Yasarla, R., Patel, V.M.: Transweather: Transformer-based restoration of images degraded by adverse weather conditions. In: Proceedings of the IEEE/CVF conference on computer vision and pattern recognition. pp. 2353–2363 (2022)
39. Wan, T., Wang, A., Ai, B., Wen, B., Mao, C., Xie, C.W., Chen, D., Yu, F., Zhao, H., Yang, J., Zeng, J., Wang, J., Zhang, J., Zhou, J., Wang, J., Chen, J., Zhu, K., Zhao, K., Yan, K., Huang, L., Feng, M., Zhang, N., Li, P., Wu, P., Chu, R., Feng, R., Zhang, S., Sun, S., Fang, T., Wang, T., Gui, T., Weng, T., Shen, T., Lin, W., Wang, W., Wang, W., Zhou, W., Wang, W., Shen, W., Yu, W., Shi, X., Huang, X., Xu, X., Kou, Y., Lv, Y., Li, Y., et al.: Wan: Open and advanced large-scale video generative models. arXiv preprint arXiv:2503.20314 (2025)
40. Wang, T., Zhang, K., Shen, T., Luo, W., Stenger, B., Lu, T.: Ultra-high-definition low-light image enhancement: A benchmark and transformer-based method. In: Proceedings of the AAAI conference on artificial intelligence. vol. 37, pp. 2654–2662 (2023)
41. Wang, X., Xie, L., Dong, C., Shan, Y.: Real-esrgan: Training real-world blind super-resolution with pure synthetic data. In: Proceedings of the IEEE/CVF international conference on computer vision. pp. 1905–1914 (2021)
42. Wiedemer, T., Li, Y., Vicol, P., Gu, S.S., Matarese, N., Swersky, K., Kim, B., Jaini, P., Geirhos, R.: Video models are zero-shot learners and reasoners. arXiv preprint arXiv:2509.20328 (2025)
43. Wu, J., Huang, T., He, C., Long, M.: Miniveo3-reasoner: Thinking with videos from open-source priors. <https://github.com/thuml/MiniVeo3-Reasoner> (2025)
44. Yang, C., Wan, H., Peng, Y., Cheng, X., Yu, Z., Zhang, J., Yu, J., Yu, X., Zheng, X., Zhou, D., et al.: Reasoning via video: The first evaluation of video models’ reasoning abilities through maze-solving tasks. arXiv preprint arXiv:2511.15065 (2025)
45. Zhang, X., Ma, J., Wang, G., Zhang, Q., Zhang, H., Zhang, L.: Perceive-ir: Learning to perceive degradation better for all-in-one image restoration. *IEEE Transactions on Image Processing* (2025)
46. Zheng, D., Wu, X.M., Yang, S., Zhang, J., Hu, J.F., Zheng, W.S.: Selective hour-glass mapping for universal image restoration based on diffusion model. In: Proceedings of the IEEE/CVF conference on computer vision and pattern recognition. pp. 25445–25455 (2024)
47. Zheng, Z., Peng, X., Yang, T., Shen, C., Li, S., Liu, H., Zhou, Y., Li, T., You, Y.: Open-sora: Democratizing efficient video production for all. arXiv preprint arXiv:2412.20404 (2024)

Appendix for V-Bridge

A Details

A.1 Training Details

Data. For the training data, we construct high-quality (HQ) and low-quality (LQ) image pairs using samples from FoundIR and RealCE. Specifically, FoundIR contains several common degradation categories, including blur, lowlight, JPEG compression, haze, rain, as well as combinations of multiple degradations. To maintain a balanced distribution, we perform uniform sampling across these degradation categories. In contrast, RealCE mainly consists of text degradation data in both Chinese and English, and its samples are treated as a single category during sampling. Unless otherwise specified in the main paper, the default training set size used in our experiments is 1K. The detailed data construction procedure can be found in Sec. 3.2.

Table 7: Training Configurations for V-Bridge.

Parameter	Value
BF16	True
Learning Rate	2e-5
LR Scheduler Type	constant_with_warmup
LR Warmup Steps	100
Adam Weight Decay	3e-2
Adam Epsilon	1e-10
Maximum Grad Norm	0.05
GPUs Per Node	8
Number of Nodes	1
Seed	42

Details. During training, the hyperparameters used in our experiments are summarized in Tab. 7. As described in Sec. 3.3, we adopt a three-stage training strategy. The primary difference across stages lies in the input video resolution, while all other training hyper-parameters remain consistent throughout the entire training process. Specifically, the three training stages use resolutions of 512, 720, and 960, respectively. The meaning of these resolutions is defined as follows. Taking 512 as an example, for each frame in the original video, we first resize the frame while preserving its aspect ratio such that the shorter side is scaled to 512. Then, a 512×512 patch is randomly cropped from the resized frame for training. The resolutions used in the other stages follow the same procedure. The total training schedule consists of 300 epochs, which are evenly divided across the three stages.

A.2 Test Details

Benchmarks. Next, we provide a detailed description of each benchmark used in our experiments, including the specific degradation types involved and their corresponding detailed information.

- **FoundIR [25].** This test set includes common degradation types such as blur, low-light, JPEG compression, haze, rain, as well as combinations of multiple degradations. It contains a total of 1,500 samples, with the majority of the data at resolutions of 1080p or higher.
- **Dense-Haze [1].** Dense-Haze comprises 33 pairs of real-world hazy and corresponding haze-free images, capturing a variety of outdoor scenes. The hazy conditions are densely distributed and visually uniform, created using professional haze machines to introduce authentic atmospheric haze.
- **UHD-LL [40].** The first real UHD low-light image enhancement dataset, featuring 4K image pairs captured under diverse conditions with different levels of darkness and noise. The dataset provides a test set consisting of 115 image pairs for evaluation purposes.
- **UAV-Rain1K [6].** This dataset is specifically designed for studying rain removal in aerial imagery captured by unmanned aerial vehicles (UAVs). It provides a comprehensive collection of images that reflect various rainy conditions and environmental scenarios. The test set consists of 220 paired images, each with an average resolution of around 1500×1000 pixels, offering sufficient detail for evaluating the performance of deraining algorithms.
- **HQ-NightRain [9].** The test portion of the dataset consists of 300 image pairs and is categorized based on the type of nighttime rain degradation into three distinct subsets: rain streaks (RS), raindrops (RD), and mixed rain (SD), which combines both streaks and drops.
- **WeatherBench [16].** This dataset contains images with snow, haze, and rain degradations. In our evaluation, we only utilize the snow subset, which provides 200 pairs of corresponding low-quality and high-quality images. It is worth noting that snow removal is an unseen task for our model, as this type of degradation is not included in the tasks encountered during training.

Inference. During inference, a unified prompt is employed across all tasks, with the full prompt details provided in Box.A.1 and A.2. Since generating high-resolution videos (e.g., 4K) directly with video generation models incurs substantial VAE decoding time, we adopt a practical approach for efficiency: frames with resolutions exceeding 2K are first resized to approximately 2K while maintaining their original aspect ratio for inference. The outputs are then rescaled back to the original resolution prior to metric computation. During generation, we use UniPC, adapted for flow matching, as the sampling scheduler with 50 sampling steps. The classifier-free guidance scale is set to 5.0, and the timestep shift is also set to 5.0.

Box A.1: Prompt for Image Restoration

A restoration-focused video strictly based on the input image. The camera is completely static with no movement, no zoom, and no rotation. The original composition, objects, layout, and perspective are preserved exactly. Focus on visual restoration and enhancement: remove noise, reduce blur, eliminate rain artifacts, remove compression artifacts, and improve clarity, sharpness, and fine details while maintaining natural textures, accurate colors, and balanced lighting. Only extremely subtle and natural temporal consistency is allowed. The video should appear stable, clean, and realistic, as if the input image has been gently restored over time.

Box A.2: Negative Prompt for Image Restoration

camera movement, panning, tilting, zooming, rotation, scene change, object movement, new objects, object deformation, style change, artistic style, illustration, painting, cartoon, over-saturated colors, overexposure, underexposure, motion blur, jitter, flickering, shaking, low quality, worst quality, noise, blur, rain, fog, compression artifacts, jpeg artifacts, aliasing, text, subtitles, watermark, logo, distorted anatomy, extra limbs, duplicated objects, exaggerated motion, creative animation

Metrics. In this work, we adopt **PSNR** and **SSIM** as evaluation metrics, where higher values indicate better performance. Following the computation methodology in FoundIR , these metrics are defined as:

1. PSNR (Peak Signal-to-Noise Ratio):

$$\text{MSE} = \frac{1}{HW} \sum_{i=1}^H \sum_{j=1}^W (I(i, j) - \hat{I}(i, j))^2, \quad (7)$$

$$\text{PSNR} = 10 \cdot \log_{10} \left(\frac{L^2}{\text{MSE}} \right) \quad (8)$$

where I and \hat{I} denote the ground-truth and reconstructed images, H and W are the height and width of the images, and L is the maximum pixel value (e.g., 255 for 8-bit images).

2. SSIM (Structural Similarity Index):

$$\text{SSIM}(I, \hat{I}) = \frac{(2\mu_I\mu_{\hat{I}} + C_1)(2\sigma_{I\hat{I}} + C_2)}{(\mu_I^2 + \mu_{\hat{I}}^2 + C_1)(\sigma_I^2 + \sigma_{\hat{I}}^2 + C_2)} \quad (9)$$

where $\mu_I, \mu_{\hat{I}}$ and $\sigma_I^2, \sigma_{\hat{I}}^2$ are the means and variances of I and \hat{I} , $\sigma_{I\hat{I}}$ is their covariance, and C_1, C_2 are stabilizing constants.

Both metrics are computed per image and averaged over the dataset to obtain the final evaluation scores.

B Additional Experimental Results

B.1 Visualization Results

We present additional visualization results in Fig.7, Fig.8, and Fig.9.

B.2 Failure Cases

We present several failure cases of our method as shown in Fig.10, along with the corresponding visualization results of FoundIR-G on the same data.

C Limitations and Future Work

This work primarily explores the feasibility of transferring the prior knowledge of video generation models to low-level vision tasks, and demonstrates the effectiveness and potential of such a transfer. However, the current approach faces two main limitations: task generalization and efficiency. In future work, we aim to extend the transfer of video generation priors to a broader range of tasks, further validating the potential of video generation models as foundation models for vision. Additionally, since the present study focuses solely on demonstrating potential, we did not incorporate any acceleration strategies to avoid confounding factors in the analysis. Moving forward, we plan to introduce acceleration techniques to make the approach practically usable in real-world scenarios.

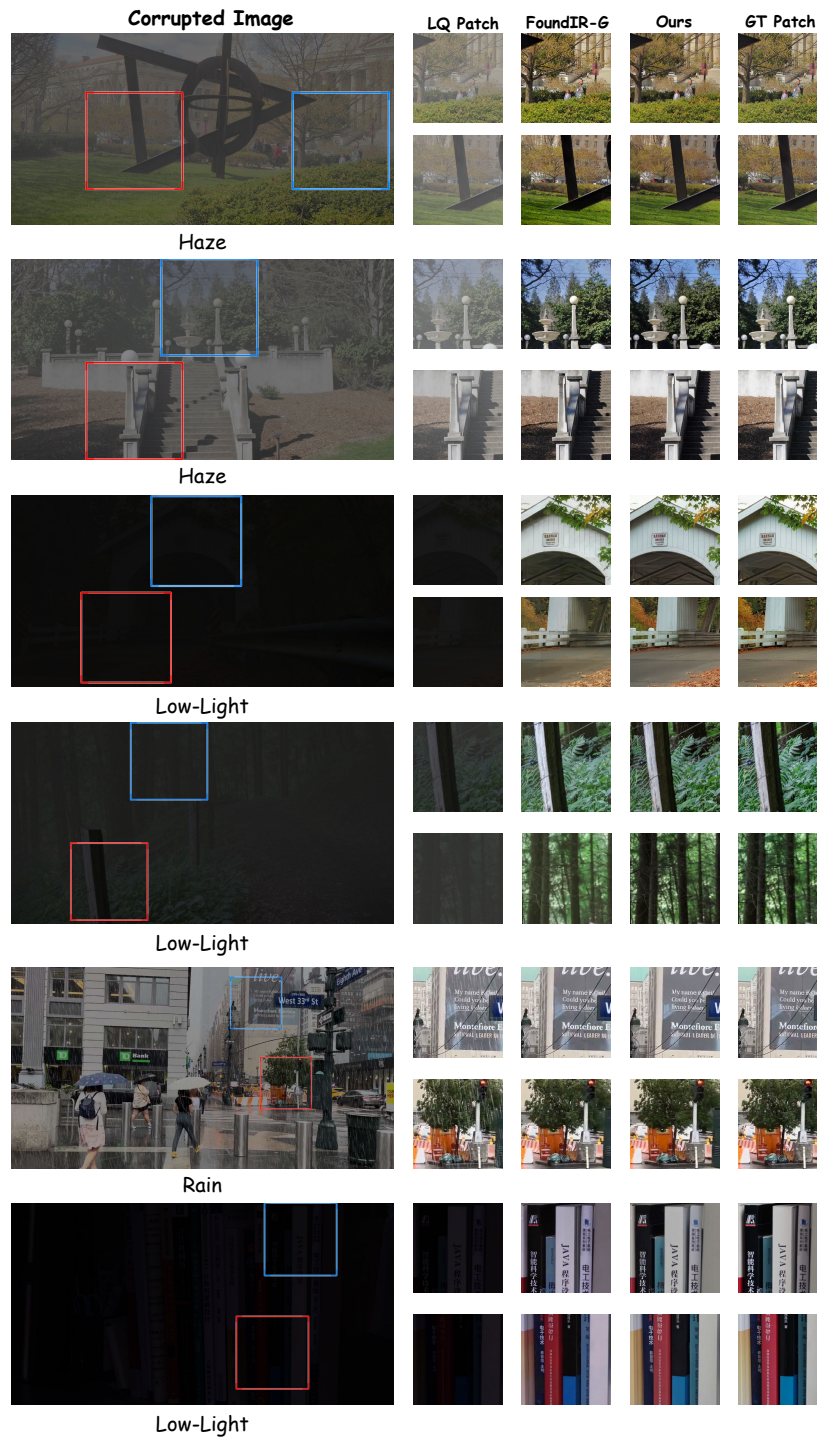


Fig. 7: Additional visualization results.

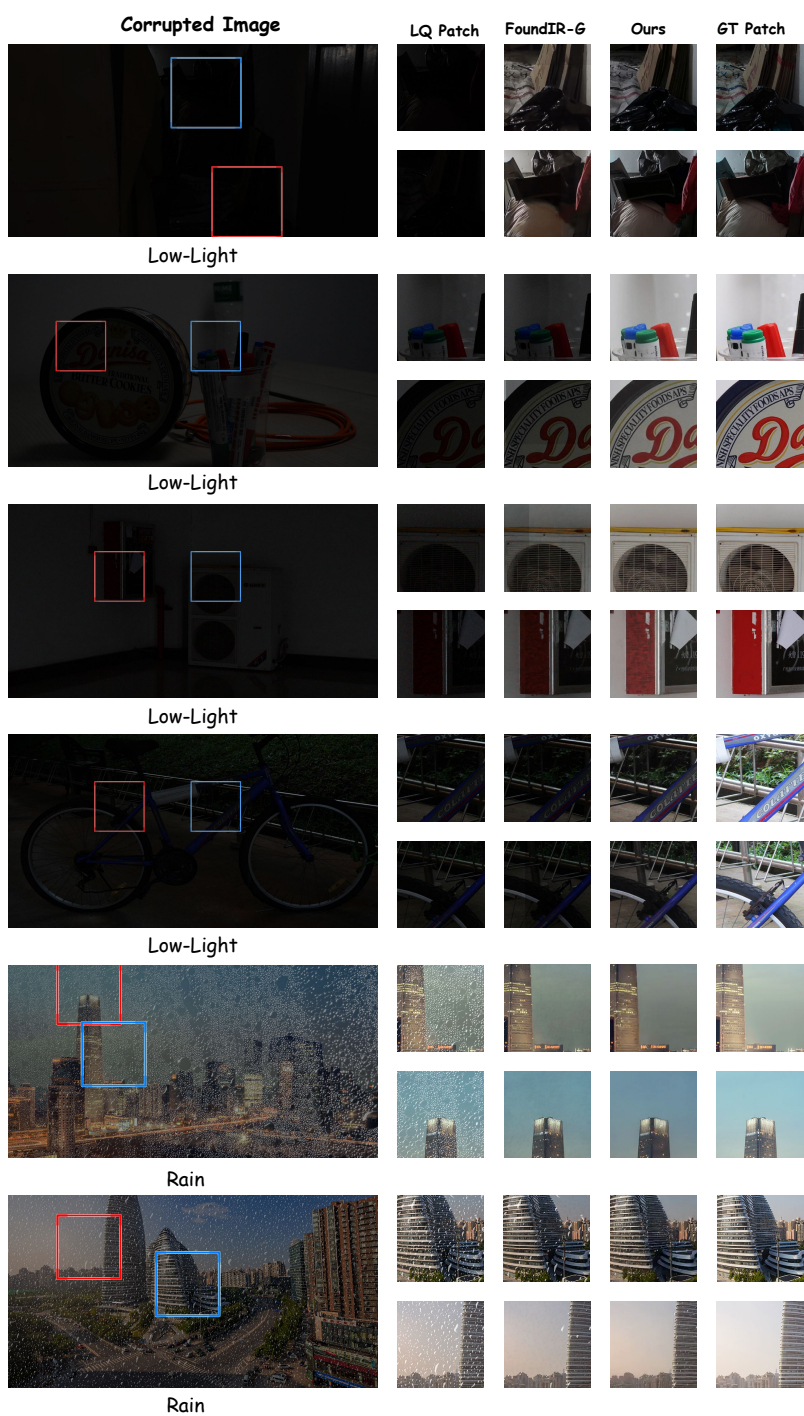


Fig. 8: Additional visualization results.

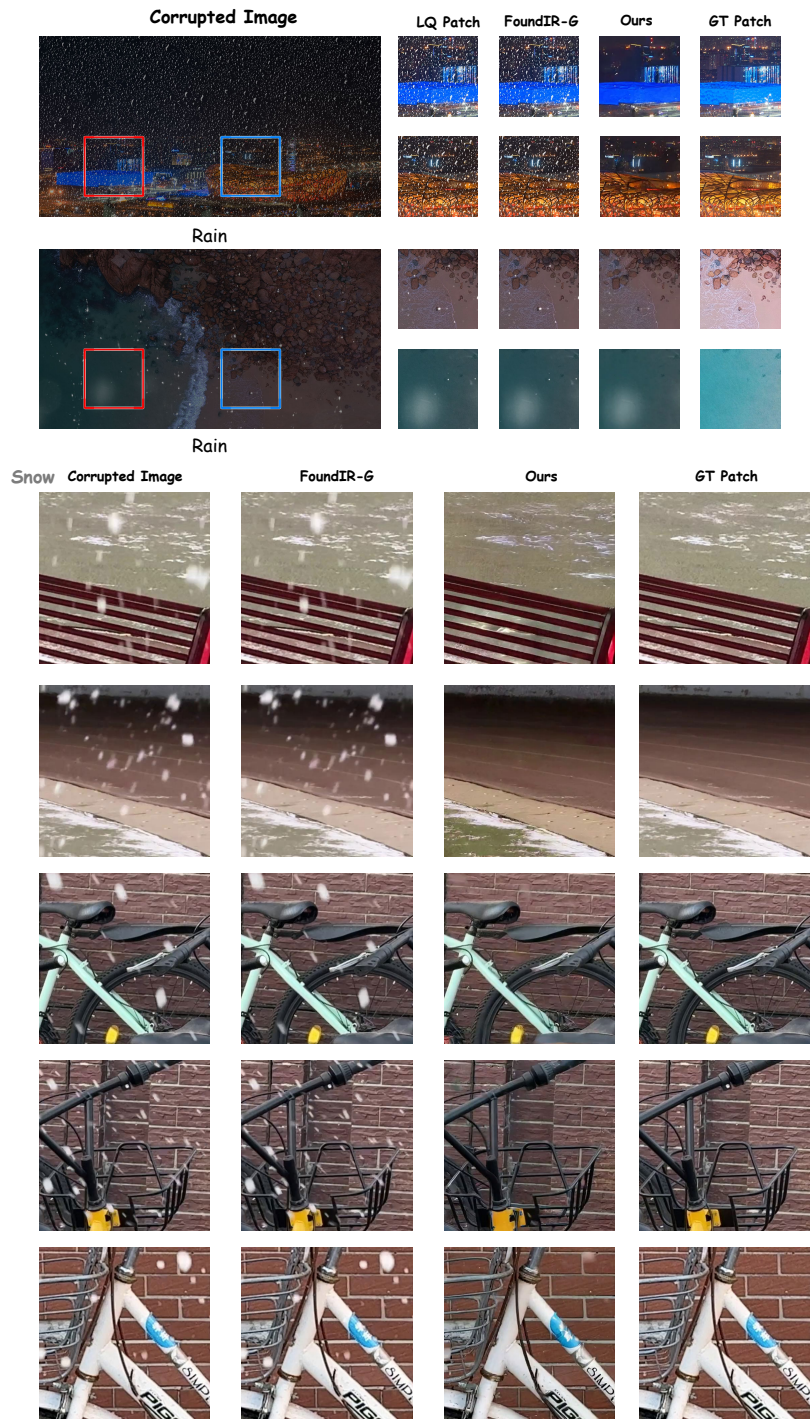


Fig. 9: Additional visualization results.

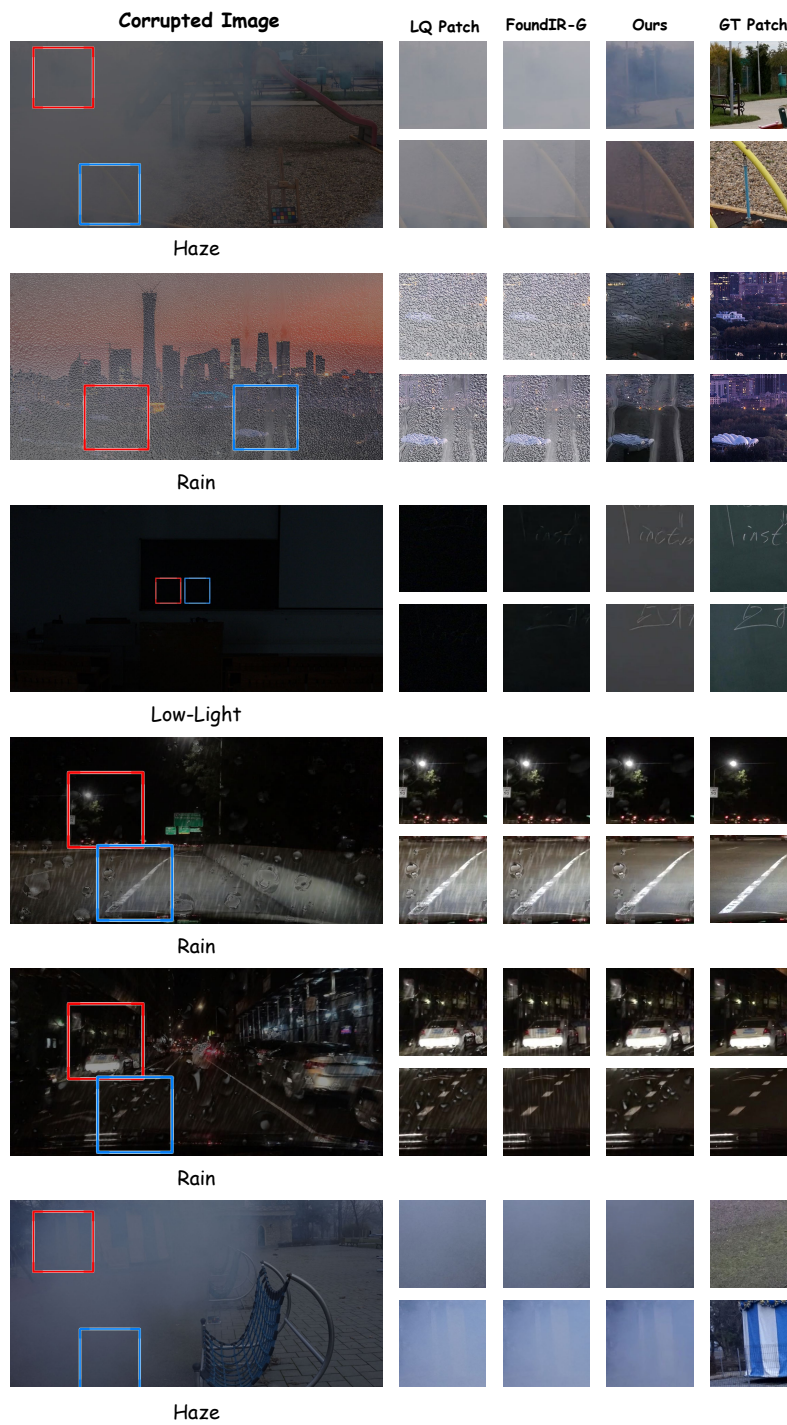


Fig. 10: Failure cases.